The Astrophysical Journal, 877:155 (12pp), 2019 June 1 https://doi.org/10.3847/1538-4357/ab14ef

A Parametric Study of the Structure of Hall Magnetic Field Based on Kinetic Simulations. I. Anti-parallel Magnetic Reconnection in an Asymmetric Current Sheet

Longlong Sang[1,2], Quanming Lu[1,2], Rongsheng Wang[1,2], Kai Huang[1,2], and Shui Wang[1,2]
[1] CAS Key Lab of Geospace Environment, School of Earth and Space Sciences, University of Science and Technology of China, Hefei 230026, People's Republic of China; qmlu@ustc.edu.cn, rswan@ustc.edu.cn
[2] CAS Center for Excellence in Comparative Planetology, People's Republic of China
Received 2019 February 3; revised 2019 March 17; accepted 2019 March 28; published 2019 June 5

Abstract

The generation of the Hall magnetic field is considered one of the most important characteristics in collisionless magnetic reconnection. Here, in this paper, with two-dimensional particle-in-cell simulations, we study the structure of the Hall magnetic field generated during anti-parallel magnetic reconnection in an asymmetric current sheet. A quadrupolar structure of the Hall magnetic field is first formed, and then it evolves into a hexapolar structure with the proceeding magnetic reconnection. In the quadrupolar structure of the Hall magnetic field, the quadrants on the side of the current sheet with the weaker magnetic field (the dominant Hall magnetic field) are much stronger than those on the other side, and they can cross the center of the current sheet. With the increase of the ratio of the magnetic fields or the decrease of the density ratio (here, the ratio is defined as the values between the side with the stronger magnetic field to that with the weaker magnetic field), the tendency will become more salient. However, with a decrease of the temperature ratio, the tendency reverses. With the proceeding reconnection, two ribbons with an enhanced Hall magnetic field are generated in the region below the dominant Hall magnetic field, and then a hexapolar structure of the Hall magnetic field is formed, which will become stronger with an increase of the ratio of the magnetic field or decrease of the density, while the effect of the temperature asymmetry is much weaker than that of the magnetic field and density asymmetry. The generation of the Hall magnetic field can be explained by the in-plane current carried mainly by the electrons.

Key words: magnetic reconnection – Sun: heliosphere

1. Introduction

The topology of magnetic field lines is rearranged during magnetic reconnection, and the stored magnetic energy in a current sheet is released into plasma kinetic energy (Parker 1957; Sweet 1958; Sato & Hayashi 1979; Sonnerup 1979; Drake et al. 2006; Angelopoulos et al. 2013; Lu et al. 2013; Burch et al. 2016). Magnetic reconnection is believed to be related to the observed explosive phenomena in the solar atmosphere (Tsuneta 1996; Somov & Kosugi 1997; Lazarian & Desiati 2010; Cheng et al. 2018), the Earth's magnetosphere (Nagai et al. 2001; Angelopoulos et al. 2008; Wang et al. 2010; Burch et al. 2016), and laboratory plasma (Stenzel & Gekelman 1981; Ji et al. 1998; Zhong et al. 2010; Dong et al. 2012; Yamada et al. 2014; Fan et al. 2019). However, plasmas in space and astrophysical environments are usually very sparse and supposed to be collisionless (Baumjohann & Treumann 1996). In collisionless reconnection, the motions of ions and electrons move in different ways, and these kinds of decoupling motions result in the Hall effect, which leads to the in-plane current in collisionless reconnection (Sonnerup 1979; Terasawa 1983; Birn et al. 2001; Hesse et al. 2001; Lu et al. 2010). The magnetic field in the out-of-plane direction, which is also called the Hall magnetic field, is then generated, and it is regarded as one of the most salient properties in collisionless magnetic reconnection (Deng & Matsumoto 2001; Ma & Bhattacharjee 2001; Nagai et al. 2001; Øieroset et al. 2001; Pritchett 2001; Shay et al. 2001; Ren et al. 2005; Wang et al. 2012).

The characteristics of a Hall magnetic field in symmetric magnetic reconnection, where physical parameters are the same on the two sides of a current sheet, have been thoroughly studied with both particle-in-cell (PIC) simulations (Shay & Drake 1998; Pritchett 2001; Fu et al. 2006; Lu et al. 2011) and satellite observations (Nagai et al. 2001; Øieroset et al. 2001; Wang et al. 2010), and the Hall magnetic field is considered to have a quadrupolar structure (Birn et al. 2001; Nagai et al. 2001). It is proposed that that kind of Hall magnetic field structure results from the in-plane Hall current carried mainly by electrons, which is directed away from the X line along the separatrix and toward the X line along the magnetic field line just below the separatrix (Nagai et al. 2003; Lu et al. 2010). In symmetric reconnection without a guide field, both the in-plane Hall current and Hall magnetic field have good symmetry, while the introduction of a guide field distorts the symmetry (Pritchett 2001; Eastwood et al. 2010; Huang et al. 2010, 2014; Lu et al. 2011; Wang et al. 2012; Lai et al. 2015; Zhou et al. 2018).

However, there is little chance of observing symmetric reconnection in nature, and most magnetic reconnection that occurs in the magnetosphere, solar atmosphere, and interplanetary space is asymmetric, meaning the physical parameters on the two sides of the current sheet are usually different. One typical example of asymmetric magnetic reconnection occurs in the Earth's magnetopause between the shocked magnetosheath and magnetosphere (Khotyaintsev et al. 2006; Mozer et al. 2008; Burch et al. 2016; Wang et al. 2017; Zhang et al. 2017). In general, the magnetic field in the magnetosphere is much stronger than that in the magnetosheath, while the plasma density in the magneosheath is much larger than that in the magnetosphere (Burch et al. 2016; Wang et al. 2017). There have been plenty of satellite observations of magnetic reconnection in the magnetopause (Mozer et al. 2008; Eriksson et al. 2015; Burch et al. 2016; Zhou et al. 2016; Peng et al. 2017; Wang et al. 2017; Zhang et al. 2017). By studying an asymmetric reconnection event

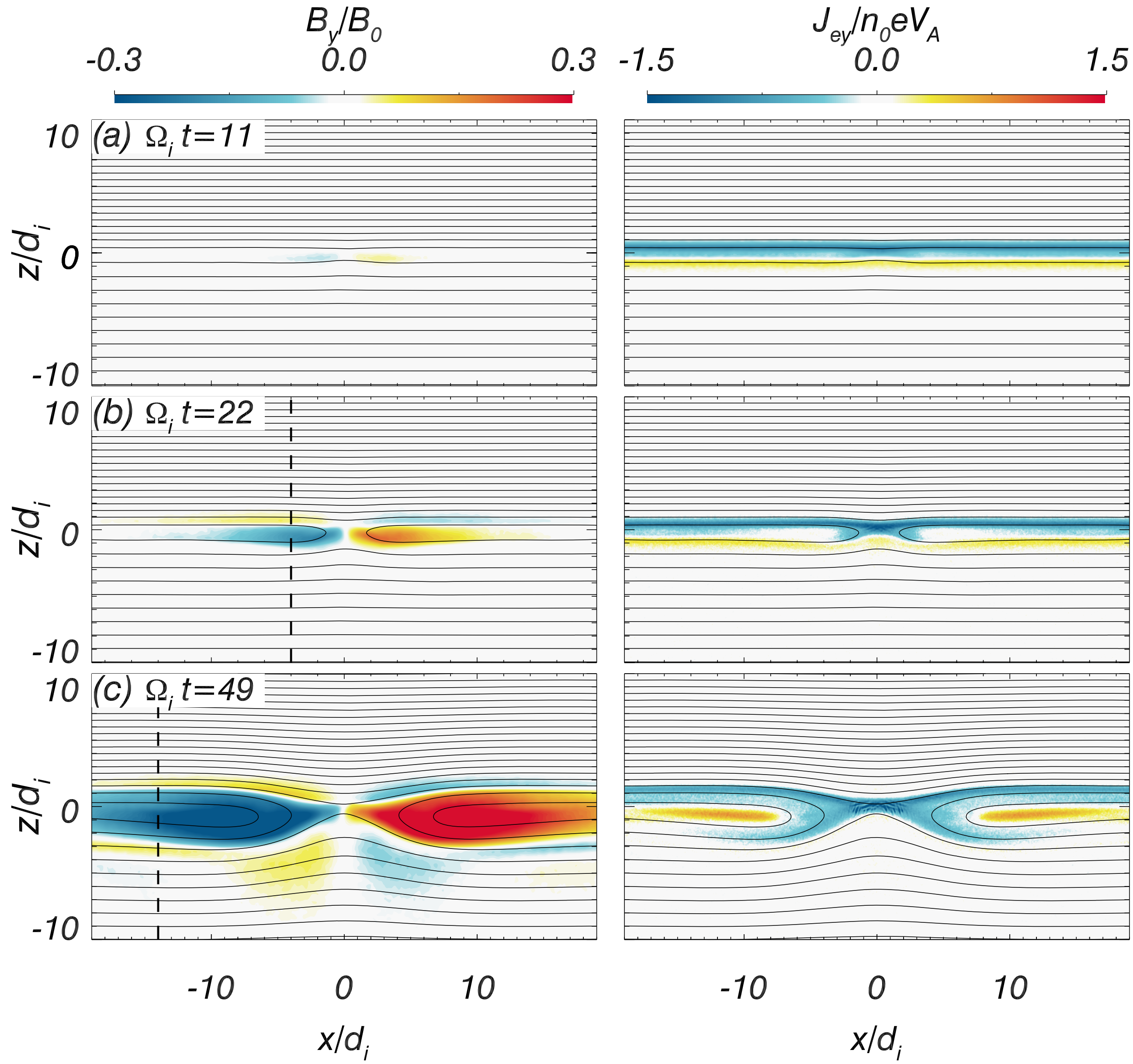

Figure 1. Hall magnetic field B_y/B_0 and electron current in the y direction ($J_{ey}/(n_0 e V_A)$) at $\Omega_i t$ = (a) 11, (b) 22, and (c) 49 for Run 1.

observed by the THEMIS satellite in the magnetopause, Mozer et al. (2008) found that the Hall magnetic field has a bipolar structure, which is developed only on the magnetosheath side. Recently, the *MMS* mission launched in 2015 fostered a wave of enthusiasm for asymmetric reconnection in the magnetopause, and the Hall magnetic field was revealed to still have a quadrupolar structure, although its size and amplitude on the magnetosheath side are much larger than those on the magnetosphere side (Zhou et al. 2016; Peng et al. 2017; Wang et al. 2017). Taking advantage of high-resolution plasma measurements, it has been verified that such a quadrupolar Hall magnetic field is produced by the Hall current sheet carried by electrons (Peng et al. 2017; Zhang et al. 2017). However, Eriksson et al. (2015) also identified a hexapolar structure of a Hall magnetic field after analyzing an asymmetric reconnection event observed by Cluster in the solar wind. PIC simulations also gave controversial conclusions regarding the structure of a Hall magnetic field in asymmetric reconnection. Both bipolar and quadrupolar structures of Hall magnetic fields have been reported in PIC simulations of asymmetric reconnection (Pritchett 2008; Pritchett & Mozer 2008; Malakit et al. 2010; Hesse et al. 2014; Huang et al. 2014; Shay et al. 2016), while Sang et al. (2018) found that the Hall magnetic field can evolve from a quadrupolar structure into a hexapolar one in their two-dimensional (2D) PIC of asymmetric reconnection without a guide field. The goal of this paper is to resolve the controversy by performing 2D PIC simulations to study the structures of Hall magnetic fields during magnetic reconnection in an asymmetric current sheet with different ratios of magnetic field, plasma density, and temperature. In this paper, we analyze in detail the structures of a Hall magnetic field formed during anti-parallel magnetic reconnection in an asymmetric current sheet. The effects of a guide field on the structures of a Hall magnetic field will be discussed in the future.

The paper is organized as follows. We describe the simulation model in Section 2, and then present the simulation results in Section 3. A summary and discussion are given in Section 4.

2. Simulation Model

In this paper, we employ a 2D PIC simulation model to investigate the structures of a Hall magnetic field during asymmetric magnetic reconnection with different conditions. In the model, the motions of ions and electrons are controlled by the Lorentz force according to Newton's second law with relativistic effects. These particles can move in the (x, z) plane, and all three velocity components of every particle are retained. The electromagnetic fields, which are defined in the grids of the (x, z) plane, are calculated by the Maxwell equations. The model has been successfully used to study collisionless magnetic reconnection in the previous work (Fu et al. 2006; Huang et al. 2010; Lu et al. 2016).

In the simulations, we use the initial equilibrium configurations of the asymmetric current sheet as described in Quest & Coroniti (1981), and the profile of the magnetic field is given as

$$\boldsymbol{B}_0(z) = B_0\left[\tanh\frac{z}{\lambda} + R\right]\boldsymbol{e}_x. \tag{1}$$

Here, λ is the half width of the current sheet. The parameter R, which is usually $|R| < 1$, is the parameter to determine the asymmetry of the magnetic field in the current sheet. The amplitude ratio of the magnetic field on both sides of the current sheet is $R_B = (1 + R)/(1 - R)$. The velocity distributions of both ions and electrons satisfy the Maxwellian function with a drift velocity in the y direction.

There are two ways to balance the magnetic pressure across the asymmetric current sheet. The first approach is to assume that the ion and electron temperatures are uniform across the current sheet, which are denoted by T_{i0} and T_{e0}, respectively. The profile of the number density is determined by

$$n(z) = n_0\left(1 - \alpha_1\tanh\frac{z}{\lambda} - \alpha_2\tanh^2\frac{z}{\lambda}\right). \tag{2}$$

In order to satisfy the pressure balance, we can get $\alpha_1 = 2\alpha_2 R$ and $\alpha_2 = B_0^2/[2\mu_0 n_0(T_{e0} + T_{i0}]$, and the corresponding density ratio is $R_n = (1 - \alpha_1 - \alpha_2)/(1 + \alpha_1 - \alpha_2)$.

The other approach is to keep the density uniform across the current sheet, which is denoted by n_0. The profile of the ion and electron temperatures satisfy

$$T_i(z) = T_{i0}\left(1 - \beta_1\tanh\frac{z}{\lambda} - \beta_2\tanh^2\frac{z}{\lambda}\right), \tag{3}$$

$$T_e(z) = T_{e0}\left(1 - \beta_1\tanh\frac{z}{\lambda} - \beta_2\tanh^2\frac{z}{\lambda}\right), \tag{4}$$

where $\beta_1 = 2\beta_2 R$ and $\beta_2 = B_0^2/[2\mu_0 n_0(T_{i0} + T_{e0})]$. The temperature ratios of both ions and electrons are $R_T = (1 - \beta_1 - \beta_2)/(1 + \beta_1 - \beta_2)$.

In this paper, the size of the simulation domain is $L_x \times L_z = 54d_i \times 22.5d_i$ (where $d_i = c/\omega_{pi}$ is the ion inertial length based on n_0) and it contains 1080×450 cells. Therefore, the spatial resolution is $\Delta x = \Delta z = 0.05d_i$. The time step is chosen as $\Delta t = 0.001\Omega_i^{-1}$ (where $\Omega_i = eB_0/m_i$ is the ion cyclotron frequency). The mass ratio of ions to electrons is $m_i/m_e = 100$, and the light speed is $c/V_A = 15$ (where $V_A = B_0/\sqrt{\mu_0 n_0 m_i}$ is the Alfvén speed based on B_0 and n_0). The

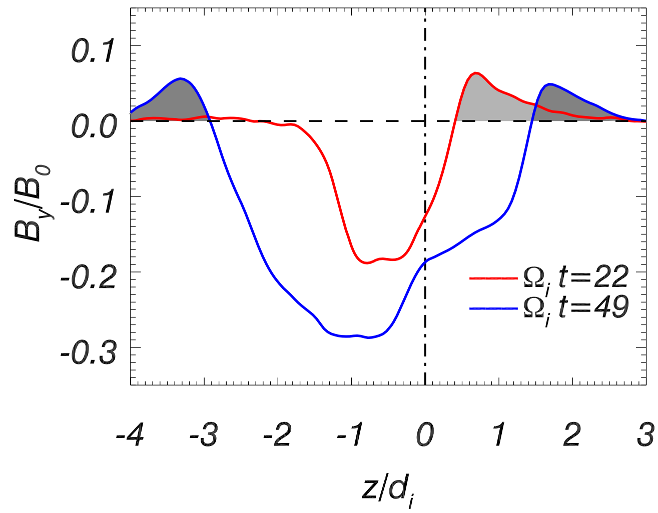

Figure 2. Cuts of the Hall magnetic field B_y/B_0 along $x = -4.0d_i$ at $\Omega_i t = 22$ and $x = -14.0d_i$ at $\Omega_i t = 49$ for Run 1, as denoted by the dashed lines in Figures 1(b) and (c), respectively.

initial temperature ratio of ions to electrons is $T_{i0}/T_{e0} = 4$. More than 10^8 particles for every species are used in the simulations. Periodic boundary conditions are employed along the x direction, while the z direction is set as the conducting boundary conditions.

3. Simulation Results

In this paper, with 2D PIC simulations we perform a parametric study of the structures of a Hall magnetic field during anti-parallel magnetic reconnection in an asymmetric current sheet, and the parameters include the density ratio (R_n), the amplitude ratio of magnetic field (R_B) and the temperature ratio (R_T), which are listed in the table below. We define the ratio as the value between the sides with a stronger magnetic field to that with a weaker magnetic field. In Runs 1–3, we consider the influence of the density ratio (R_n), and the effects of the amplitude ratio of the magnetic field (R_B) are investigated in Runs 4–5, while Runs 6–8 focus on the influence of the temperature ratio (R_T).

Run	R_B	R_n	R_T
1	2	1/3	…
2	2	1/6	…
3	2	1/10	…
4	3	1/3	…
5	4	1/3	…
6	2	…	2/5
7	2	…	1/2
8	2	…	1/3

We at first describe in detail the simulation results of Run 1. Figure 1 shows the Hall magnetic field B_y/B_0 and electron current in the y direction $(J_{ey}/(n_0eV_A)$ at $\Omega_i t$ = (a) 11, (b) 22, and (c) 49. Magnetic reconnection occurs at about $\Omega_i t = 9$, and in the vicinity of the X line the Hall magnetic field starts to appear and the electron current is enhanced. With the proceeding of the magnetic reconnection, the Hall magnetic field begins to form an obvious structure around $\Omega_i t = 12$. At first, the Hall magnetic field has a quadrupolar structure, whose size and amplitude in the lower part of the current sheet are

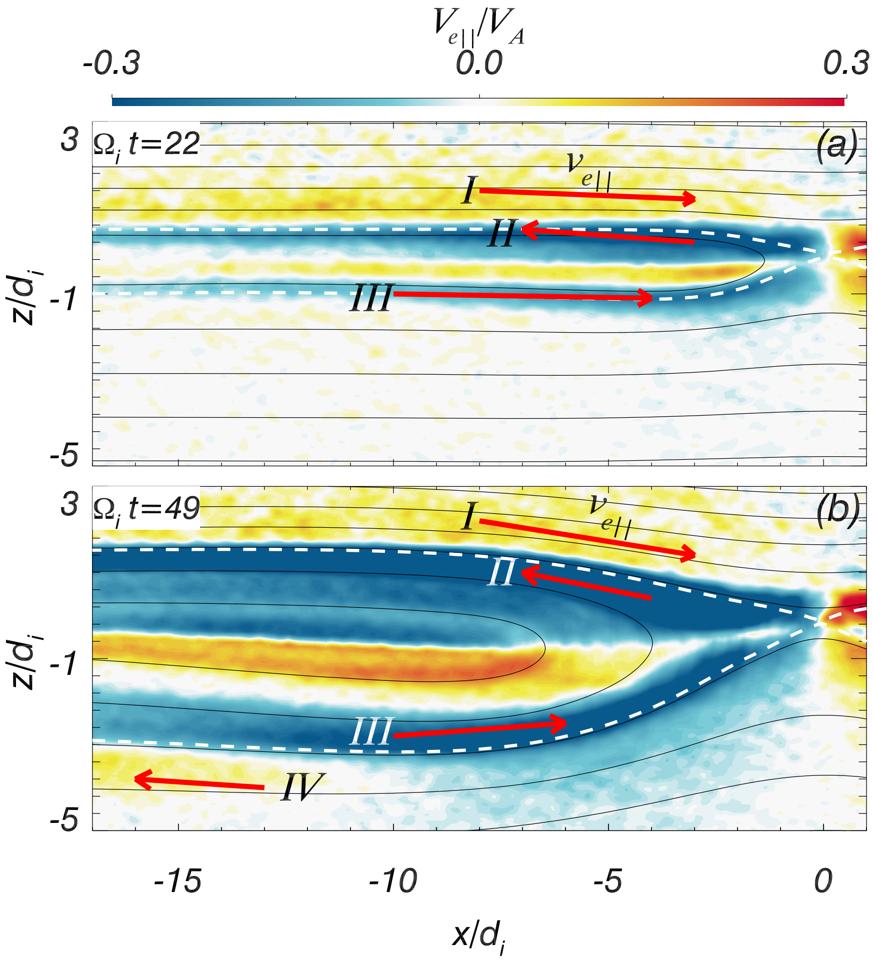

Figure 3. Electron bulk velocity parallel to the in-plane magnetic field ($V_{e||}/V_A$) at $\Omega_i t$ = (a) 22 and (b) 49 for Run 1.

much bigger than those in the upper part, as demonstrated in Figure 1(b). Then, both the size and amplitude of the quadrupolar B_y structure increase with time. Around $\Omega_i t = 26$, below the quadrupolar structure of the Hall magnetic field, two ribbons with an enhanced out-of-plane magnetic field are generated, then they are continually enhanced as the reconnection evolves. Finally, the Hall magnetic field possesses a hexapolar structure. This can be seen more clearly in Figure 2, which plots the cuts of the Hall magnetic field B_y/B_0 along $x = -4.0d_i$ at $\Omega_i t = 22$ and $x = -14.0d_i$ at $\Omega_i t = 49$ for Run 1, as denoted by the dashed lines in Figures 1(b) and (c), respectively. At $\Omega_i t = 22$, the Hall magnetic field has a quadrupolar structure, and it is directed toward the $-y$ direction in the lower part of the current sheet, while in the upper part it is pointed toward the y direction. The out-of-plane magnetic field with a negative value can cross the center of the current sheet ($z = 0$). At $\Omega_i t = 49$, another region with an enhanced Hall magnetic field pointing in the y direction, is generated around $z = -3.3d_i$, and now the Hall magnetic field has a hexapolar structure.

In order to explain the generation mechanism for B_y structures in asymmetric magnetic reconnection. In Figure 3, we show the electron bulk velocity parallel to the in-plane magnetic field ($V_{e||}/V_A$) at $\Omega_i t$ = (a) 22 and (b) 49 for Run 1. Because the in-plane magnetic field is pointed toward the $+x$ direction in the upper part of the current sheet and the $-x$ direction in the lower part, it is easy to see that the electrons around the separatrix region in the upper part of the current sheet (denoted by II in the figure) move away from the X line, and are directed toward the X line around the separatrix region in the lower part of the current sheet (denoted by III in the figure). Just above the separatrix region II there exists an electron flow directed toward the X line along the magnetic field (denoted by I in the figure). At $\Omega_i t = 49$, there still exist other electron flows away from the X line along the magnetic field just below the separatrix in the lower part of the current sheet (denoted by IV in the figure). The in-plane current is mainly contributed by electrons; the resulting in-plane current sheet generated by such an electron flow will lead to the generation of the Hall magnetic field described in Figure 1.

Next, we will investigate the dependence of the Hall magnetic field on the ratios of magnetic field and density between the two sides of the current sheet.

3.1. The Influence of the Density Ratio R_n

Figures 4(a)–(c) show the Hall magnetic field B_y/B_0 for Runs 1–3. The selected times are $\Omega_i t = 21$ for Run 1, $\Omega_i t = 22$ for Run 2, and $\Omega_i t = 23$ for Run 3. At these times, the reconnected magnetic flux is $0.3V_A B_0$ for all three runs. Obviously, the Hall magnetic field in Runs 1–3 exhibits a

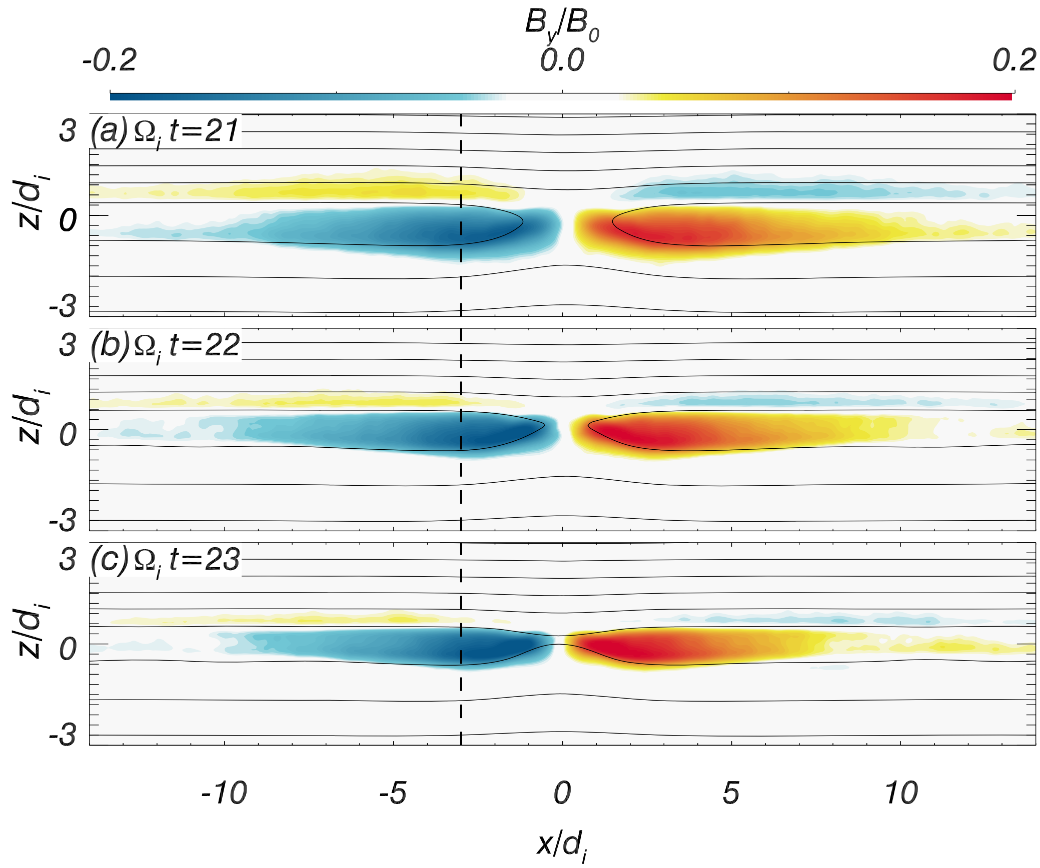

Figure 4. Hall magnetic field B_y/B_0 for Runs 1–3. The selected times are $\Omega_i t = 21$ for (a) Run 1, $\Omega_i t = 22$ for (b) Run 2, and $\Omega_i t = 23$ for (c) Run 3. At these times, the reconnected magnetic flux is $0.3V_AB_0$ for all three runs.

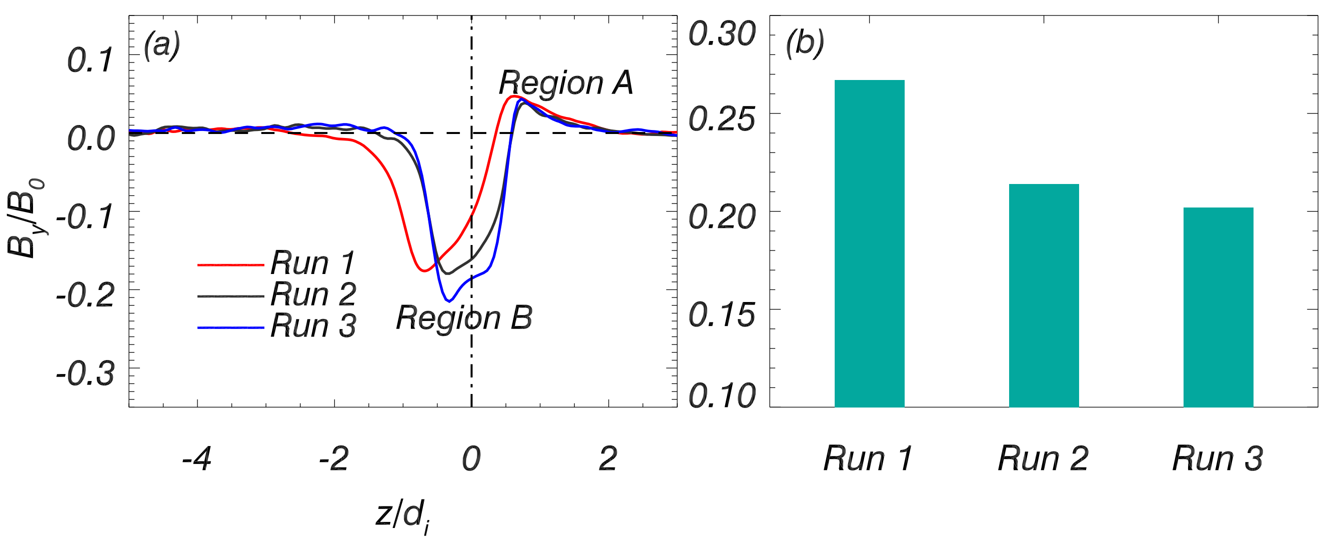

Figure 5. (a) Cut of the Hall magnetic field along $x = -3.0d_i$ for Runs 1–3 (denoted by the dashed line in Figure 4) at the same times as in Figure 4. (b) Ratio of peak amplitudes between Regions A and B (cyan bars). Here, the Hall magnetic fields in Regions A and B have positive and negative values, respectively.

quadrupolar structure at these times. Figure 5(a) plots the cut of the Hall magnetic field along $x = -3.0d_i$ for Runs 1–3 (denoted by the dashed line in Figure 4) at the same times as in Figure 4, and (b) is the ratio of peak amplitudes between Regions A and B. Here, the Hall magnetic fields in Regions A and B have positive and negative values, respectively. We can find that with the decrease of R_n, which is the density ratio between the two sides of the current sheet, the amplitude of the Hall magnetic field in Region B increases, while the amplitude of the Hall magnetic field in Region A tends to decrease. Therefore, with the decrease of R_n, the ratio of peak amplitudes between Regions A and B decreases. Note that the Hall magnetic field in Region B can cross the center of the current sheet ($z = 0$) for all three runs.

Figures 6(a)–(c) show the Hall magnetic field B_y/B_0 for Runs 1–3. The selected times are $\Omega_i t = 32$ for Run 1, $\Omega_i t = 42$

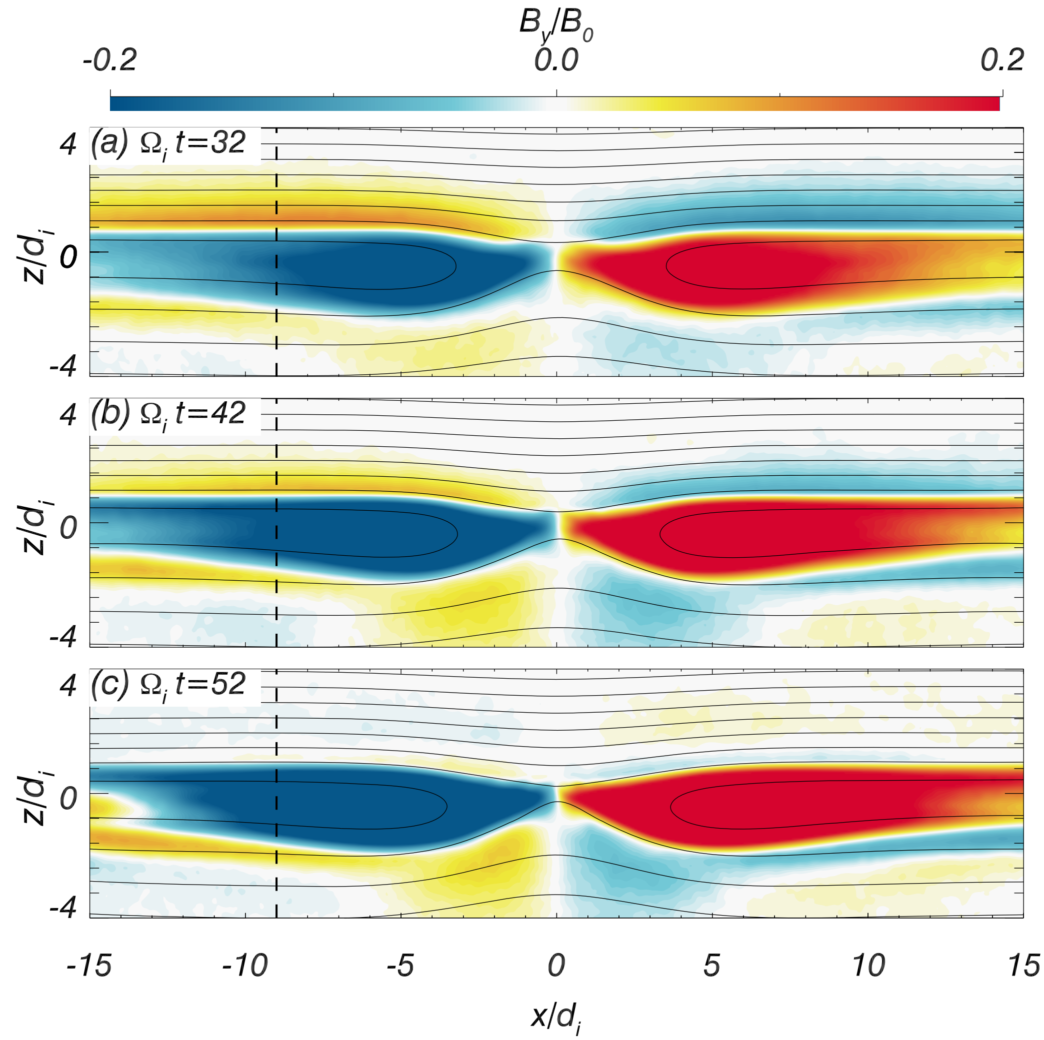

Figure 6. Hall magnetic field B_y/B_0 for Runs 1–3. The selected times are $\Omega_i t = 32$ for (a) Run 1, $\Omega_i t = 42$ for (b) Run 2, and $\Omega_i t = 52$ for (c) Run 3. At these times, the reconnected magnetic fluxes are the same for all three runs, which is $0.9V_A B_0$.

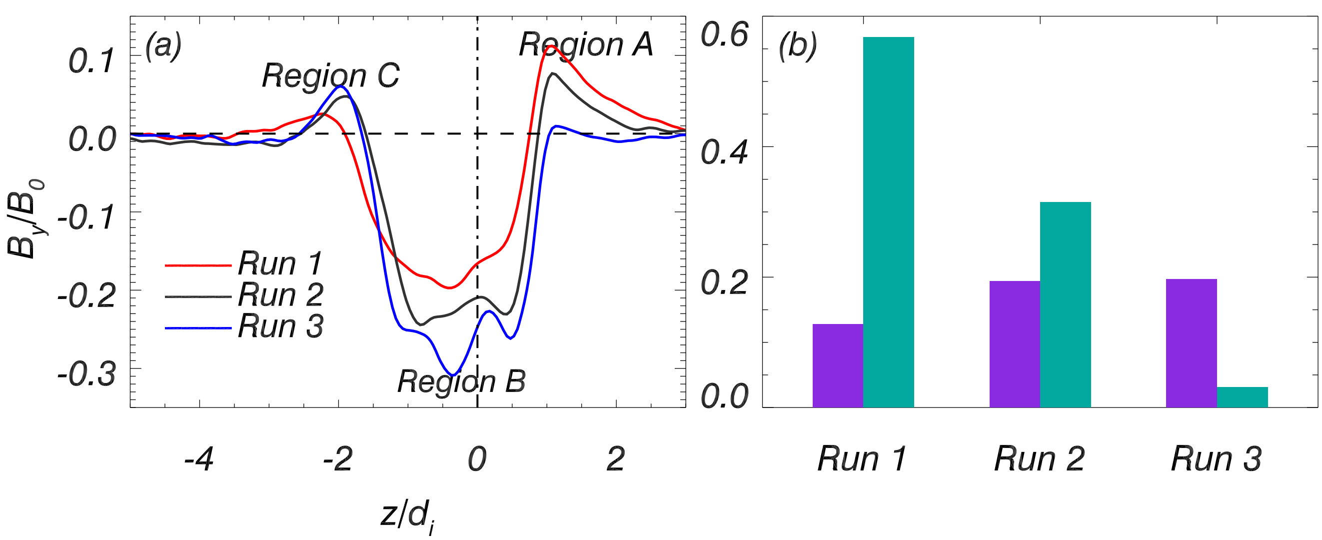

Figure 7. (a) Cut of the Hall magnetic field along $x = -9.0d_i$ for Runs 1–3 at the same times as in Figure 6. (b) Ratio of peak amplitudes between Regions A and B (cyan bars), and the ratio between Regions C and B (purple bars). Here, the Hall magnetic field in Region C has a positive value.

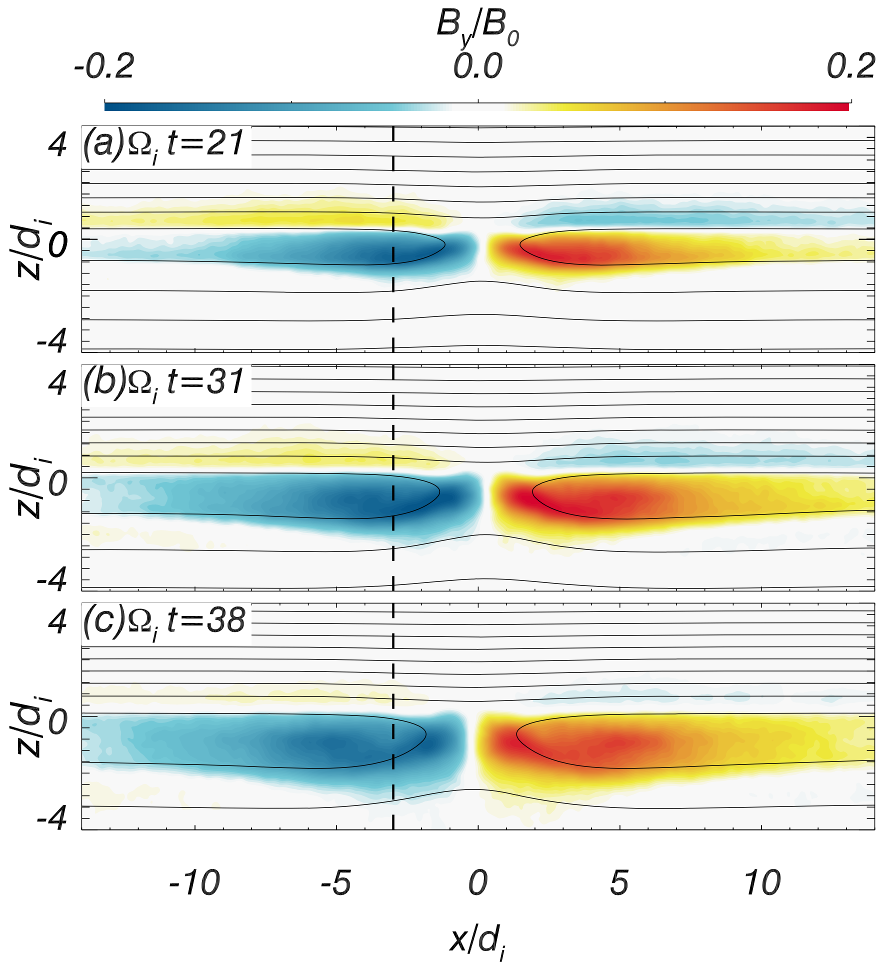

Figure 8. Hall magnetic field B_y/B_0 for Runs 1, 4, and 5. The selected times are $\Omega_i t = 21$ for (a) Run 1, $\Omega_i t = 31$ for (b) Run 4, and $\Omega_i t = 38$ for (c) Run 5. At these times, the reconnected magnetic flux is $0.3V_AB_0$ for all three runs.

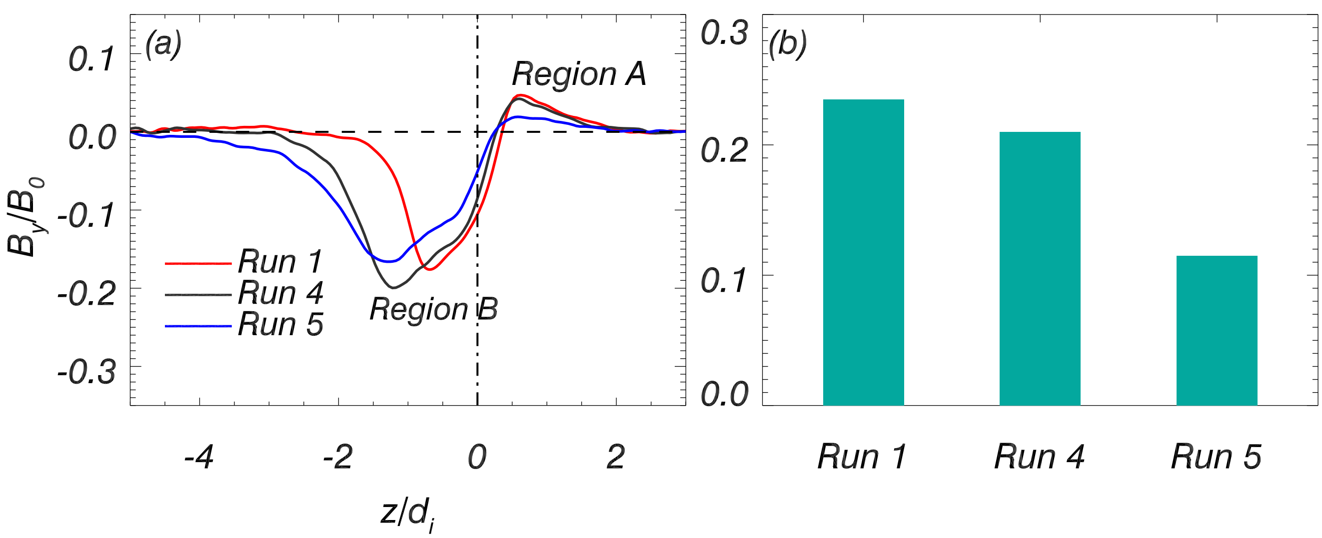

Figure 9. (a) Cut of the Hall magnetic field along $x = -3.0d_i$ for Runs 1, 4, and 5 at the same times as in Figure 8. (b) Ratio of peak amplitudes between Regions A and B (cyan bars).

for Run 2, and $\Omega_i t = 52$ for Run 3. At these times, the reconnected magnetic fluxes are the same for all three runs, which is $0.9V_AB_0$. Obviously, the Hall magnetic field exhibits a hexapolar structure, which is described in Figure 1(c). Figure 7(a) plots the cut of the Hall magnetic field along $x = -9.0d_i$ for Runs 1–3 at the same times as in Figure 6, and (b) plots the ratio of peak amplitudes between Regions A and B, and the ratio between Regions C and B. Here, the Hall

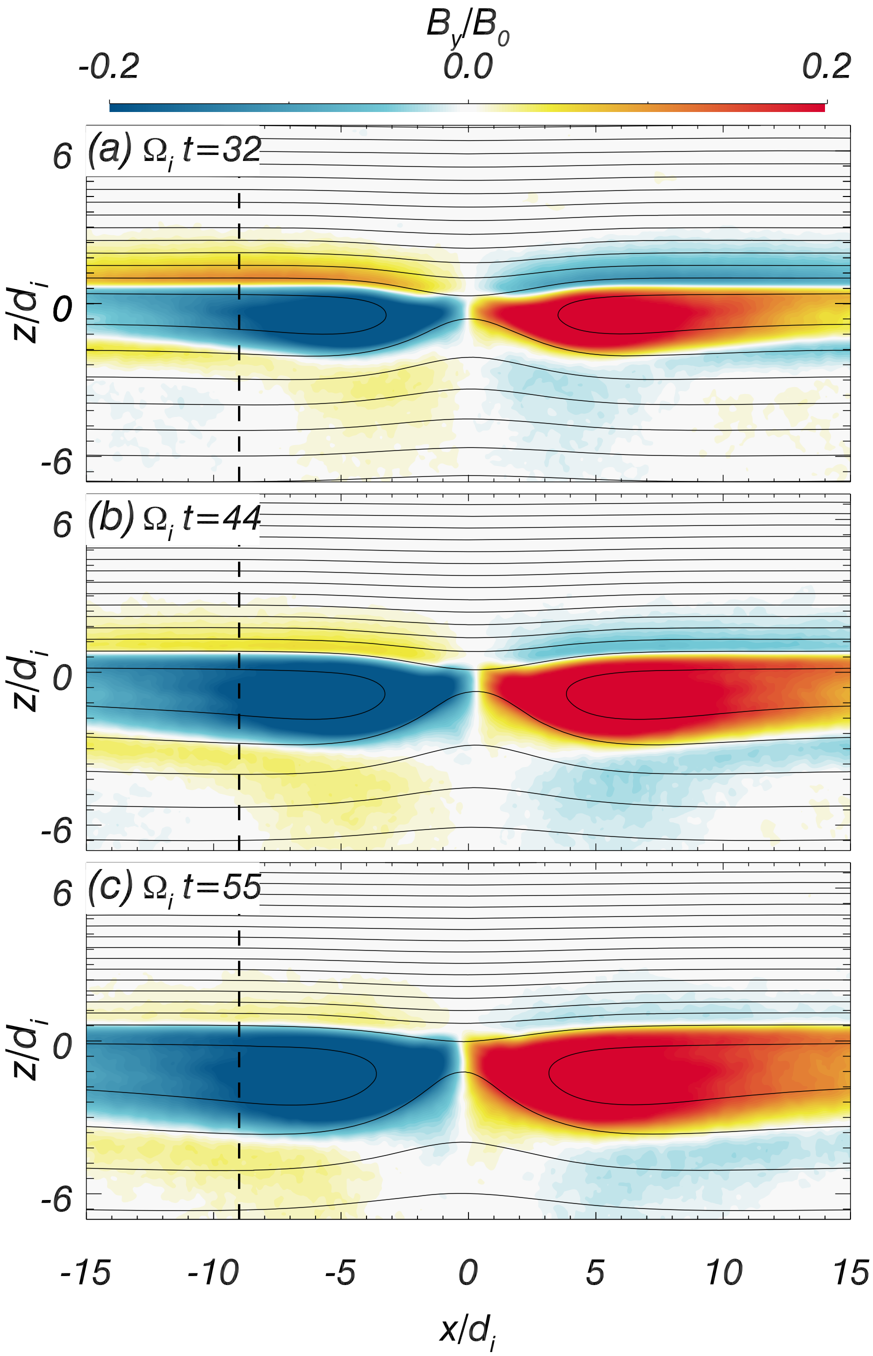

Figure 10. Hall magnetic field B_y/B_0 for Runs 1, 4, and 5. The selected times are $\Omega_i t = 32$ for (a) Run 1, $\Omega_i t = 44$ for (b) Run 4, and $\Omega_i t = 55$ for (c) Run 3. At these times, the reconnected magnetic flux is $1.0 V_A B_0$ for all three runs.

magnetic field in Region C has a positive value. With the decrease of R_n, the amplitude of the Hall magnetic field in Region B and Region C increases, while the amplitude of the Hall magnetic field in Region A decreases. Therefore, with the decrease of R_n, the ratio of peak amplitude between Regions A and B decreases, and that between C and B increases.

3.2. The Influence of the Magnetic Field Ratio R_B

Figures 8(a)–(c) show the Hall magnetic field B_y/B_0 for Runs 1, 4, and 5. The selected times are $\Omega_i t = 21$ for Run 1, $\Omega_i t = 31$ for Run 4, and $\Omega_i t = 38$ for Run 5. At these times, the reconnected magnetic flux is $0.3 V_A B_0$ for all three runs. Obviously, the Hall magnetic field in Runs 1, 4, and 5 exhibits a quadrupolar structure. Figure 9(a) plots the cut of the Hall magnetic field along $x = -3.0 d_i$ for Runs 1, 4, and 5 at the same times as in Figure 8, and (b) is the ratio of peak amplitudes between Regions A and B. With the increase of R_B, which is the magnetic field ratio between the two sides of the current sheet, the peak amplitudes of the Hall magnetic field in Region B change a bit, while the peak amplitude of the Hall magnetic field in Region A decreases. Therefore, with the increase of R_B, the ratio of peak amplitudes between Regions A and B decreases. Also, the Hall magnetic field in Region B can cross the center of the current for all three runs.

Figures 10(a)–(c) show the Hall magnetic field B_y/B_0 for Runs 1, 4, and 5. The selected times are $\Omega_i t = 32$ for Run 1,

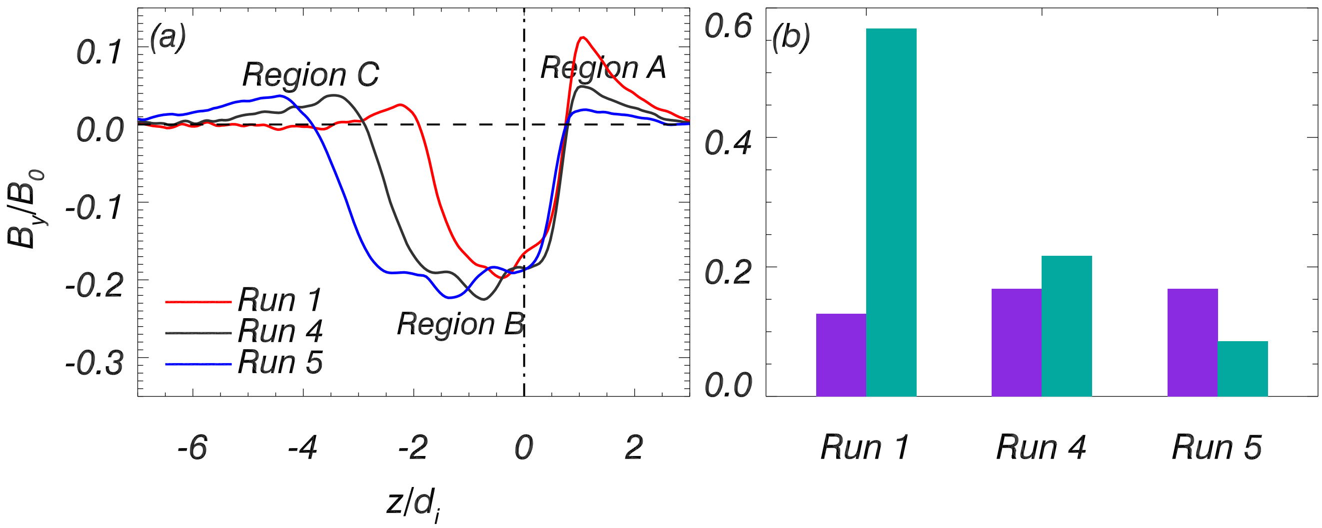

Figure 11. (a) Cut of the Hall magnetic field along $x = -9.0d_i$ for Runs 1, 4, and 5 at the same times as in Figure 10. (b) Ratio of peak amplitudes between Regions A and B (cyan bars), and the ratio between Regions C and B (purple bars).

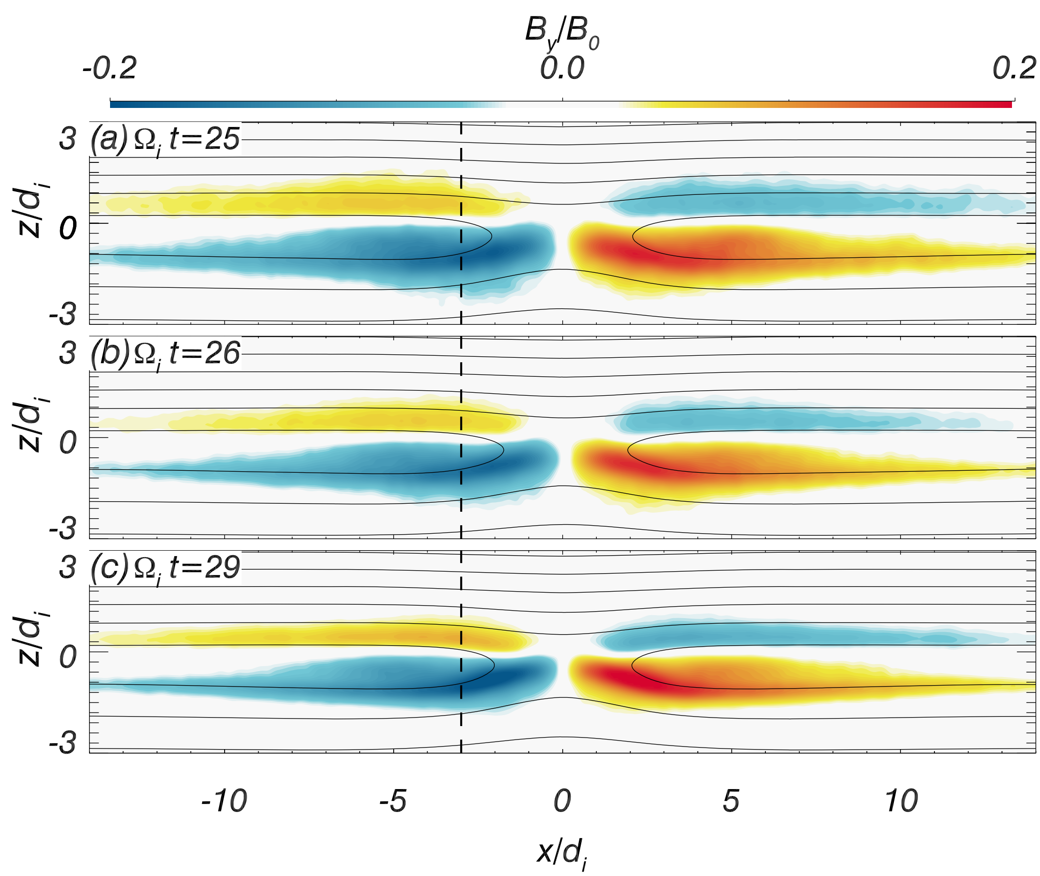

Figure 12. Hall magnetic field B_y/B_0 for Runs 6–8. The selected times are $\Omega_i t = 25$ for (a) Run 6, $\Omega_i t = 26$ for (b) Run 7, and $\Omega_i t = 29$ for (c) Run 8. At these times, the reconnected magnetic flux is $0.3V_A B_0$ for all three runs.

$\Omega_i t = 44$ for Run 4, and $\Omega_i t = 55$ for Run 3. At these times, the reconnected magnetic flux is $1.0V_A B_0$ for all three runs. Obviously, the Hall magnetic field exhibits a hexapolar structure. Figure 11(a) plots the cut of the Hall magnetic field along $x = -9.0d_i$ for Runs 1, 4, and 5 at the same times as in Figure 10, and (b) plots the ratio of peak amplitudes between Regions A and B, and the ratio between Regions C and B. With the increase of R_B, the peak amplitudes of the Hall magnetic field in Region B change little, while the peak amplitude of the Hall magnetic field in Region A decreases and that in Region C increases. Therefore, with the increase of R_B, the ratio of peak amplitude between Region A and B decreases and that between C and B increases.

3.3. The Influence of the Temperature Ratio $\boldsymbol{R}_{\mathrm{T}}$

Figures 12(a)–(c) show the Hall magnetic field B_y/B_0 for Runs 6–8. The selected times are $\Omega_i t = 25$ for Run 6, $\Omega_i t = 26$

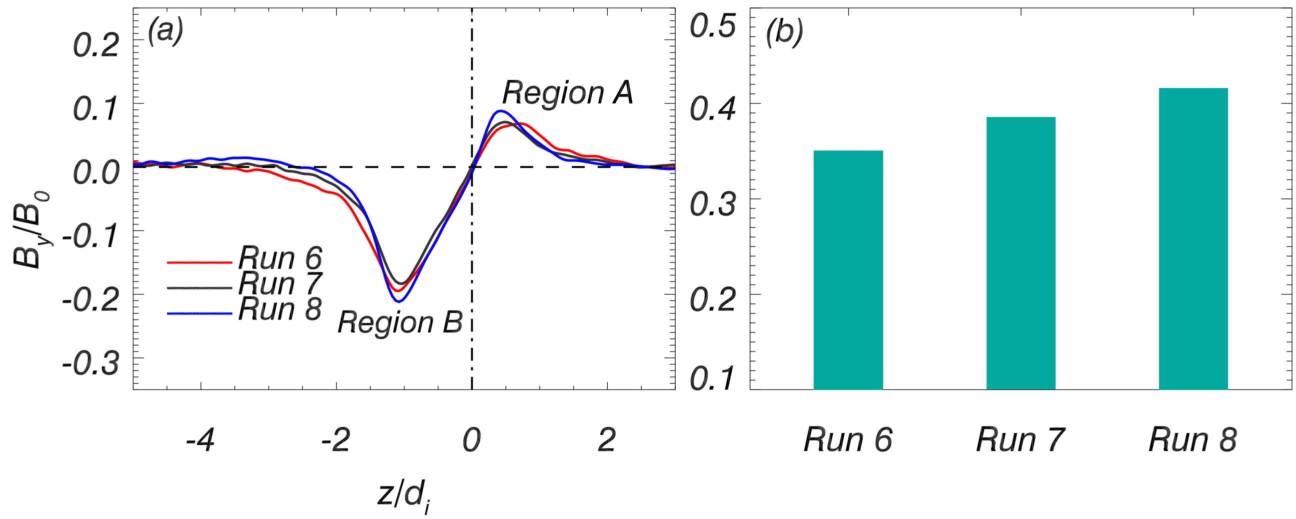

Figure 13. (a) Cut of the Hall magnetic field along $x = -3.0d_i$ for Runs 6–8 at the same times as in Figure 12. (b) Ratio of peak amplitudes between Regions A and B (cyan bars).

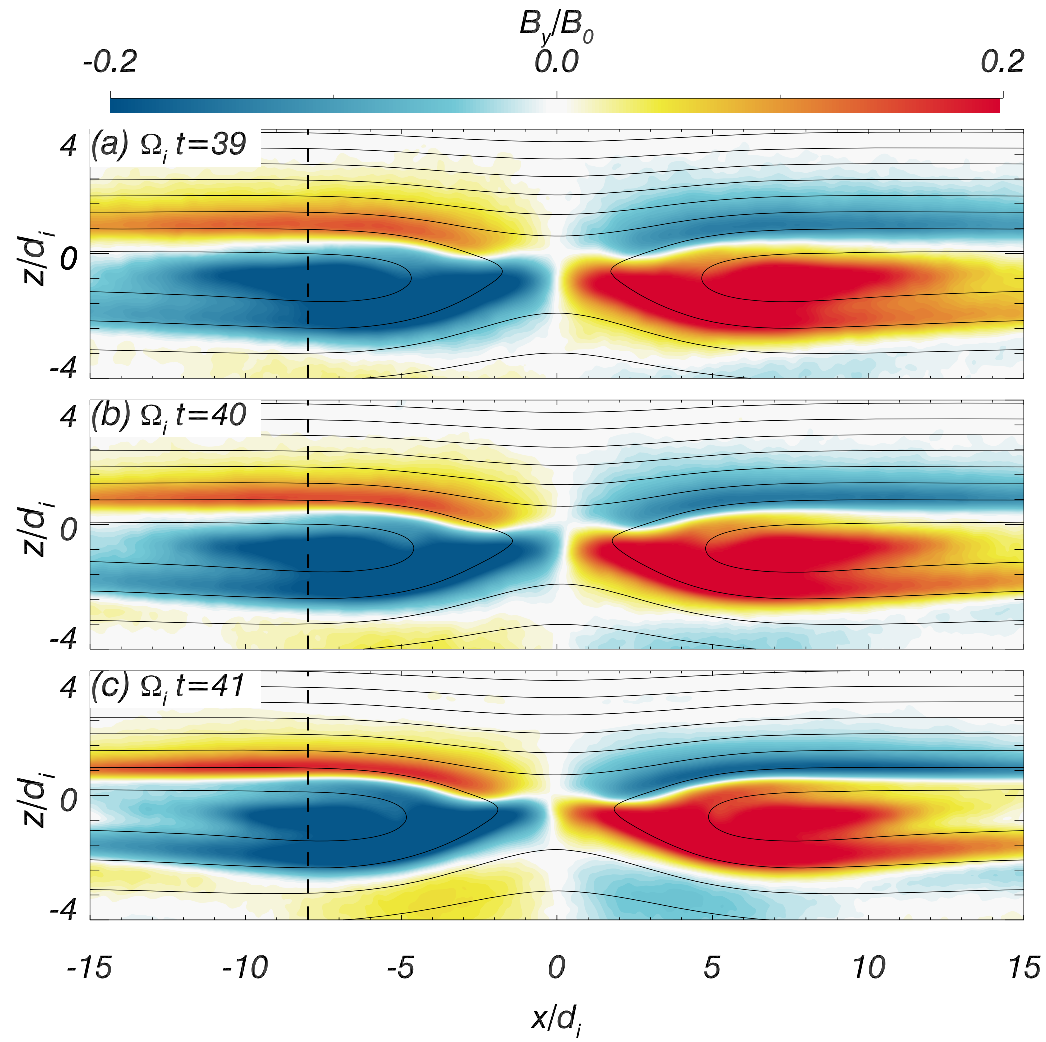

Figure 14. Hall magnetic field B_y/B_0 for Runs 6–8. The selected times are $\Omega_i t = 39$ for (a) Run 6, $\Omega_i t = 40$ for (b) Run 7, and $\Omega_i t = 41$ for (c) Run 8. At these times, the reconnected magnetic flux is $1.0V_AB_0$ for all three runs.

for Run 7, and $\Omega_i t = 29$ for Run 8. At these times, the reconnected magnetic flux is $0.3V_AB_0$ for all three runs. Obviously, the Hall magnetic field in Runs 6–8 exhibits a quadrupolar structure. Figure 13(a) plots the cut of the Hall magnetic field along $x = -3.0d_i$ for Runs 6–8 at the same times as in Figure 12, and (b) is the ratio of peak amplitudes

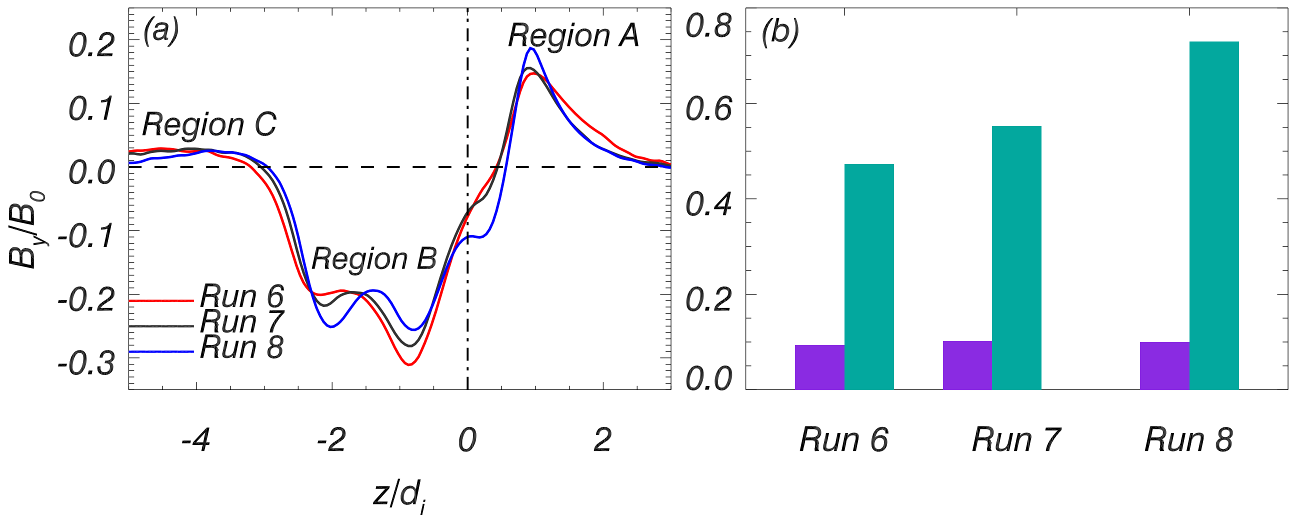

Figure 15. (a) Cut of the Hall magnetic field along $x = -8.0d_i$ for Runs 6–8 at the same times as in Figure 14. (b) Ratio of peak amplitudes between Regions A and B (cyan bars), and the ratio between Regions C and B (purple bars).

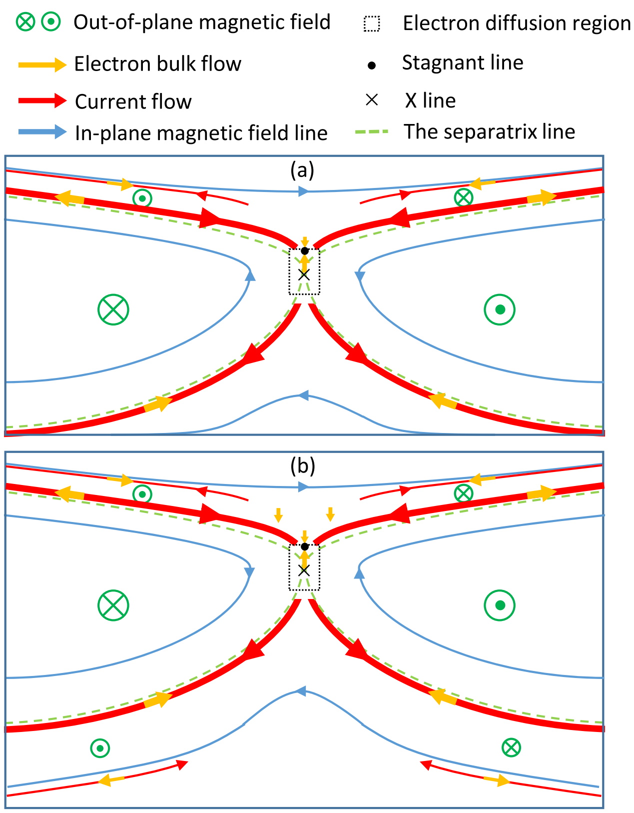

Figure 16. Diagrammatic sketch of the in-plane current system and the magnetic field structure (a) at the first stage (a quadrupolar structure of a Hall magnetic field) and (b) at the second stage (a hexapolar structure of Hall magnetic field).

between Regions A and B. We find that with the decrease of R_T, which is the temperature ratio between the two sides of the current sheet, the peak amplitudes of the Hall magnetic fields in both Regions A and B increase slightly. However, the ratio of peak amplitudes between Regions A and B increases slightly.

Figures 14(a)–(c) show the Hall magnetic field B_y/B_0 for Runs 6–8. The selected times are $\Omega_i t = 39$ for Run 6, $\Omega_i t = 40$ for Run 7, and $\Omega_i t = 41$ for Run 8. At these times, the reconnected magnetic flux is $1.0V_A B_0$ for all three runs. Obviously, the Hall magnetic field exhibits a hexapolar structure. Figure 15(a) plots the cut of the Hall magnetic field along $x = -8.0d_i$ for Runs 6–8 at the same times as in Figure 14, and (b) plots the ratio of peak amplitudes between Regions A and B, and the ratio between Regions C and B. With the decrease of R_T, the ratio of peak amplitude between Regions A and B increases slightly, and that between C and B almost does not change.

4. Summary and Discussion

In this paper, 2D PIC simulations are employed to investigate the evolution of the Hall magnetic field during anti-parallel reconnection in an asymmetric current sheet. We can identify two obvious stages of the Hall magnetic structure. In the first stage, the Hall magnetic field has a quadrupolar structure, and the quadrants on the side of the current with the weaker magnetic field magnetic field (the dominant Hall magnetic field) are much stronger than those on the other side. Differing from the Hall magnetic field generated during anti-parallel reconnection in a symmetric current sheet, the dominant Hall magnetic field can cross the center of the current sheet. Either the increase of R_B or the decrease of R_n will aggravate this tendency, while the tendency is reversed with a decrease of R_T. This kind of quadrupolar structure of the Hall magnetic field can be explained by the in-plane current system carried mainly by electrons (shown in Figure 16(a)): the electrons move to the X line along the separatrix in the lower part of the current sheet, and move away from the X line along the separatrix in the upper part; there still exists an electron flow toward the X line along the magnetic field just above the upper separatrix.

In the second stage, another electron flow moving away from the X line along the magnetic field below the separatrix in the lower part of the current sheet begins to appear. The formed in-plane current sheet system (shown in Figure 16(b)) will result in the enhancement of the out-of-plane magnetic field in the region below the dominant Hall magnetic field. It will become stronger and stronger with the increase of R_B or the decrease of R_n, while the effect of the temperature asymmetry is much weaker than that of the magnetic field and density asymmetry. The Hall magnetic field at this stage has a hexapolar structure.

Because it is one of the critical signatures of collisionless magnetic reconnection, the generation and structure of the Hall magnetic field have been studied widely. Since its 2015 launch, the *MMS* spacecraft has crossed the Earth's magnetopause many times, giving us many chances to analyze in detail the structure of the Hall magnetic field during asymmetric magnetic reconnection. The observed Hall magnetic field is revealed to have a quadrupolar or hexapolar structure. Our simulations have shown that the Hall magnetic field during anti-parallel reconnection in the asymmetric currents at first forms a quadrupolar structure and then evolves into a hexapolar structure. Therefore, the quadrupolar and hexapolar structures observed by the *MMS* spacecraft should manifest when the spacecraft observes magnetic reconnection in the Earth's magnetopause during its different stages.

This work was supported by the NSFC grants 41527804, 41774169, and the Key Research Program of Frontier Sciences, CAS(QYZDJ-SSW-DQC010). Simulations were performed on TH-1A at the National Super-Computer Center in Tianjin.

ORCID iDs

Quanming Lu https://orcid.org/0000-0003-3041-2682

References

Angelopoulos, V., McFadden, J. P., Larson, D., et al. 2008, Sci, 321, 931
Angelopoulos, V., Runov, A., Zhou, X. Z., et al. 2013, Sci, 341, 6153
Baumjohann, W., & Treumann, R. A. 1996, Basic Space Plasma Physics (London: Imperial College Press), 72
Birn, J., Drake, J. F., Shay, M. A., et al. 2001, JGR, 106, 3715
Burch, J. L., Torbert, R. B., Phan, T. D., et al. 2016, Sci, 352, 6290
Cheng, X., Li, Y., Wan, L. F., et al. 2018, ApJ, 866, 64
Deng, X. H., & Matsumoto, H. 2001, Natur, 410, 557
Dong, Q. L., Wang, S. J., Lu, Q. M., et al. 2012, PhRvL, 108, 215001
Drake, J. F., Swisdak, M., Che, H., & Shay, M. A. 2006, Natur, 443, 553
Eastwood, J. P., Shay, M. A., Phan, T. D., & Øieroset, M. 2010, PhRvL, 104, 205001
Eriksson, S., Lapenta, G., Newman, D. L., et al. 2015, ApJ, 805, 43
Fan, F. B., Xie, J. L., Zhang, Q. F., Sang, L. L., & Ding, W. X. 2019, ChPhL, 36, 015201
Fu, X. R., Lu, Q. M., & Wang, S. 2006, PhPl, 13, 012309
Hesse, M., Aunai, N., Sibeck, D., & Birn, J. 2014, GeoRL, 41, 8673
Hesse, M., Birn, J., & Kuznetsova, M. 2001, JGR, 106, 3721
Huang, C., Lu, Q., Lu, S., Wang, P. R., & Wang, S. 2014, JGR, 119, 798
Huang, C., Lu, Q., & Wang, S. 2010, PhPl, 17, 072306
Ji, H. T., Yamada, M., Hsu, S., & Kulsrud, R. 1998, PhRvL, 80, 3256
Khotyaintsev, Yu. V., Vaivads, A., Retino, A., et al. 2006, PhRvL, 97, 205003
Lai, X. S., Zhou, M., Deng, X. H., et al. 2015, ChPhL, 32, 095202
Lazarian, A., & Desiati, P. 2010, ApJ, 722, 188
Lu, Q. M., Huang, C., Xie, J. L., et al. 2010, JGR, 115, A11208
Lu, S., Angelopoulos, V., & Fu, H. S. 2016, JGR, 121, 9483
Lu, S., Lu, Q. M., Huang, C., et al. 2011, ChSBu, 56, 48
Lu, S., Lu, Q. M., Huang, C., & Wang, S. 2013, PhPl, 20, 061203
Ma, Z. W., & Bhattacharjee, A. 2001, JGR, 106, 3773
Malakit, K., Shay, M. A., Cassak, P. A., & Bard, C. 2010, JGR, 115, A10223
Mozer, F. S., Angelopoulos, V., Bonnell, J., et al. 2008, GeoRL, 35, L17S04
Nagai, T., Shinohara, I., Fujimoto, M., et al. 2001, JGR, 106, 25,929
Nagai, T., Shinohara, I., Fujimoto, M., et al. 2003, JGR, 108, 1357
Øieroset, M., Phan, T. D., Fujimoto, M., et al. 2001, Natur, 412, 414
Øieroset, M., Phan, T. D., & Fujimoto, M. 2004, GeoRL, 31, L12801
Parker, E. N. 1957, JGR, 62, 509
Peng, F. Z., Fu, H. S., Cao, J. B., et al. 2017, JGR, 122, 6349
Pritchett, P. L. 2001, JGR, 106, 3783
Pritchett, P. L. 2008, JGR, 113, A06210
Pritchett, P. L., & Mozer, F. S. 2008, JGR, 114, A11210
Quest, K. B., & Coroniti, F. V. 1981, JGR, 86, 3289
Ren, Y., Yamada, M., Gerhardt, S., et al. 2005, PhRvL, 95, 055003
Sang, L. L., Lu, Q. M., Wang, R. S., et al. 2018, PhPl, 25, 062120
Sato, T., & Hayashi, T. 1979, PhFl, 22, 1189
Shay, M. A., & Drake, J. F. 1998, GeoRL, 25, 3759
Shay, M. A., Drake, J. F., & Rogers, B. N. 2001, JGR, 106, 3759
Shay, M. A., Phan, T. D., Haggerty, C. C., et al. 2016, GeoRL, 43, 4145
Somov, B., & Kosugi, T. 1997, ApJ, 485, 859
Sonnerup, B. U. Ö. 1979, Space Plasma Physics: Magnetic Field Reconnection Vol. 3 (Amsterdam: North Holland), 46
Stenzel, R. L., & Gekelman, W. 1981, JGR, 86, 649
Sweet, P. A. 1958, in IAU Symp. 6, Electro-magnetic Phenomena in Cosmical Physics, ed. B. Lehnert (Cambridge: Cambridge Univ. Press), 123
Terasawa, T. 1983, GeoRL, 10, 475
Tsuneta, S. 1996, ApJ, 456, 840
Wang, R. S., Lu, Q. M., Huang, C., & Wang, S. 2010, JGR, 115, A01209
Wang, R. S., Nakamura, R., Lu, Q. M., et al. 2012, JGR, 117, A07223
Wang, R. S., Nakamura, R., Lu, Q. M., et al. 2017, PhRvL, 118, 175101
Yamada, M., Yoo, J., Jara-Almonte, J., et al. 2014, NatCo, 5, 4774
Zhang, Y. C., Lavraud, B., Dai, L., et al. 2017, JGR, 122, 5277
Zhong, J. Y., Li, Y. T., Wang, X. G., et al. 2010, NatPh, 6, 984
Zhou, M., Ashour-Abdalla, M., Berchem, J., et al. 2016, GeoRL, 43, 4808
Zhou, M., Berchem, J., Walker, R. J., et al. 2018, JGR, 123, 1834